Journal of Colloid and Interface Science 463 (2016) 317–323

Contents lists available at ScienceDirect

Journal of Colloid and Interface Science

journal homepage: www.elsevier.com/locate/jcis

Editor's Choice

Droplet evaporation on a horizontal substrate under gravity field by mesoscopic modeling

Chiyu Xie [a], Jianying Zhang [b], Volfango Bertola [c], Moran Wang [a,*]

[a] Department of Engineering Mechanics and CNMM, Tsinghua University, Beijing 100084, China
[b] College of Engineering, Peking University, Beijing 100874, China
[c] School of Engineering, University of Liverpool, Brownlow Hill, Liverpool L69 3GH, UK

HIGHLIGHTS

- A novel evaporation scheme introduced to the multiphase LBM model for the numerical framework.
- A new method proposed to determine the critical drop size of gravity effect.
- Critical diameter of water drop is independent of evaporation conditions, and surface wettability for normal cases.

GRAPHICAL ABSTRACT

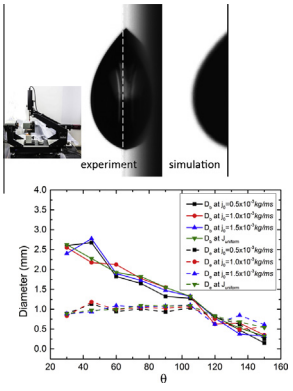

ARTICLE INFO

Article history:
Received 9 September 2015
Accepted 21 October 2015
Available online 24 October 2015

Keywords:
Drop evaporation
Gravity effect
Critical size
Lattice Boltzmann method

ABSTRACT

The evaporation of water drop deposited on a horizontal substrate is investigated using a lattice Boltzmann method (LBM) for multiphase flows with a large-density ratio. To account for the variation of evaporation flux distribution along the drop interface, a novel evaporation scheme is introduced into the LBM framework, and validated by comparison with experimental data. We aim at discovering the effect of gravity on the evaporating drop in detail, and various evaporation conditions are considered as well as different wetting properties of the substrates. An effective diameter is introduced as an indicator of the critical drop size under which gravity is negligible. Our results show that such critical diameter is much smaller than the capillary length, which has been widely accepted as the critical size in previous and current works. The critical diameter is found to be almost independent of the evaporation conditions and the surface wettability. A correlation between this critical diameter and the capillary length is also proposed for easy use in applications.

1. Introduction

Evaporation of a liquid drop on a solid substrate is a common phenomenon in everyday life, such as inkjet printing [1], accidental drippings on a hot surface [2], and the well-known "coffee-stain" effect [3–5]. As recent applications such as particle synthesis [6], DNA/RNA arrangement [7] and medical diagnostics [8] emerge, this phenomenon has gained more and more attention.

The evaporation process has been extensively discussed [9], including the shape morphology, the evaporation flux distribution and the internal flow patterns of drops. For a pure sessile droplet, there are three evaporation modes [10–13]: constant contact area (contact line pinning) mode, constant contact angle mode, and

* Corresponding author.
E-mail address: mrwang@tsinghua.edu.cn (M. Wang).

http://dx.doi.org/10.1016/j.jcis.2015.10.054
0021-9797/

both-changing mode. Along with this, evolution rules of contact angle and contact diameter or other shape properties were investigated for hydrophilic [14–20] or hydrophobic [21–26] surfaces. As for the spatial distribution of the evaporation flux, an enhancement near the contact edge was predicted for a hydrophilic drop by theoretical models [3,5,27] and numerical simulations [28–33], which is also confirmed by some experimental measurements [34–36]. In addition, the flow pattern inside drops was found to be strongly interrelated with the evaporation flux [37,38]. Most of these studies considered drops of smaller size than the capillary length, $L_c = \sqrt{\sigma/(\rho_L f_g)}$, (2.7 mm for water droplets), where σ is the surface tension, ρ_L the liquid density and f_g the gravity acceleration, hence the gravity effect was assumed to be negligible [21,39]. However, since the capillary length is usually calculated using properties at equilibrium, it may not be entirely appropriate in case of a strongly non-equilibrium process such as drop evaporation.

This work aims to reveal the impact of gravity on drop evaporation by mesoscopic modeling. In the last two decades, the lattice Boltzmann method (LBM) has become a powerful numerical scheme for fluid flow because of its advantages in dealing efficiently with complicated boundaries and interfacial transport dynamics [40–43]. Various LBM models have been developed for multiphase hydrodynamics, including the color-fluid model proposed by Gunstensen et al. [44,45], the pseudo-potential model proposed by Shan and Chen [46,47], the free-energy model by Swift et al. [48] and the mean-field model by He et al. [49,50]. Although these methods worked for some cases, they suffered from numerical instabilities for large density ratio and large viscosity ratio. Consequently, two types of models for large density ratio were developed by Zheng et al. [51] and Inamuro et al. [52,53] respectively. Both models improved the capability to deal with density ratios up to 1000 or more. It was reported that Zheng's model was more efficient and easy to implement than the Inamuro's model, and the latter met some challenges for incompressible flows [51]. Very recently, a few LBM studies [54–56] have focused on evaporation; however, the evaporation flux under gravity has never been investigated so far.

In this work, we study the evaporation of water drops deposited on a horizontal substrate by LBM simulations with special focus on the effects of gravity. We develop a numerical approach within the framework of LBM to account for evaporation regularities. After validation, the steady-state drop shapes at different scales under gravity are compared for different drop wettabilities and different evaporation modes. We introduce a critical characteristic diameter during evaporation under gravity to determine when gravity effects become significant, in alternative to the standard capillary length.

2. Numerical methods

2.1. The multiphase LBM model

The LBM model based on the free-energy scheme is adopted in this work proposed by Zheng et al. [51] for multiphase flows with large density ratios. Here, we will briefly introduce the main scheme of this model. Two distribution functions f_i and g_i are introduced to account for hydrodynamics and interfacial dynamics, respectively. The evolution equations are given as

$$f_i(\boldsymbol{x}+\boldsymbol{c_i}\Delta t, t+\Delta t) - f_i(\boldsymbol{x},t) = -\frac{1}{\tau_f}\left(f_i(\boldsymbol{x},t) - f_i^{eq}(\boldsymbol{x},t)\right) + \frac{3\Delta t\omega_i \boldsymbol{c_{i\alpha}}(\mu\partial_\alpha\phi + n\boldsymbol{G})}{c^2}, \quad (1)$$

$$g_i(\boldsymbol{x}+\boldsymbol{c_i}\Delta t, t+\Delta t) - g_i(\boldsymbol{x},t) = -\frac{1}{\tau_g}\left(g_i(\boldsymbol{x},t) - g_i^{eq}(\boldsymbol{x},t)\right), \quad (2)$$

where the subscript α is for the spatial coordinates, i is the direction of discrete velocities $\mathbf{c_i}$; ω_i is the related weight coefficient, Δt is the time step, τ_f and τ_g are the relaxation times; the macroscopic variable $\mathbf{G}$ is the acceleration of body force, $n = \frac{\rho_A+\rho_B}{2}$ is the average density, $\phi = \frac{\rho_A-\rho_B}{2}$ is the order parameter to distinguish phases A and B with density ρ_A and ρ_B respectively; μ is the chemical potential with the expression of

$$\mu = a(4\phi^3 - 4\phi^{*2}\phi) - \kappa\Delta\phi, \quad (3)$$

where ϕ^* is the maximum order parameter. The term $\mu\partial_\alpha\phi$ in Eq. (1) correlates to the Laplace pressure caused by interface actions. a and κ are two coefficients related to the interface tension σ as

$$a = (3\sigma)/(4W\phi^{*4}), \quad (4)$$

$$\kappa = (3\sigma W)/(8\phi^{*2}), \quad (5)$$

where W is the interface width.

By using the Chapman–Enskog expansion, Eqs. (1) and (2) can recover the Navier–Stokes equation and the convective Cahn–Hilliard equation [57] at a second-order accuracy. Noticing that the convective Cahn–Hilliard equation ($\partial_t\phi + (\boldsymbol{u}\cdot\nabla)\phi = M\nabla^2\mu$) is used for interface capturing and can describe flows with large density ratios well, Zheng's model can deal with large-density-ratio multiphase flows successfully.

2.2. Evaporation flux distribution

Consider a sessile drop evaporating on a horizontal substrate, as shown in Fig. 1. The evaporation flux rate along the droplet surface is the first concern for studies of microscopic behavior of drop evaporation. A uniform evaporation flux rate at the liquid–gas interface is the easiest and straightforward assumption, but it is not valid for most cases. Based on molecular kinetic theories and other capillary theories, there is a general consensus about the main features of the evaporation flux and its dependence on the position, which are summarized in Ref. [39].

When $\theta < 90°$, the local evaporation mass flux $J(r,t)$ is not uniform and a widely used correlation was given by Hu and Larson [28] as

$$J(r,t) = j_0\frac{g(\theta)}{R}\left(1-\left(\frac{r}{R}\right)^2\right)^{-\lambda} \quad \lambda = \frac{\pi-2\theta}{2\pi-2\theta} \quad (6a)$$

$$g(\theta) = (0.27\theta^2 + 1.30)\left(0.6381 - 0.2239\left(\theta - \frac{\pi}{4}\right)^2\right), \quad (6b)$$

where j_0 is the evaporation parameter, related to the vapor diffusivity D (m^2/s), the saturated vapor concentration c_V (kg/m^3), and the relative humidity H as

$$j_0 = Dc_V(1-H). \quad (6c)$$

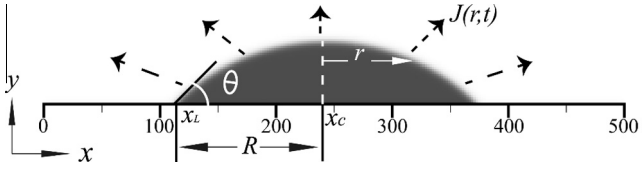

Fig. 1. Physical model of a sessile droplet evaporating on a horizontal substrate. θ is the contact angle, R is the base radius, r is the distance to the drop axis, x_c is the coordinate of droplet center, x_L is the coordinate of contact line on the left edge, and $J(r,t)$ is the local evaporation mass flux.

For $\theta = 90°$, the distribution is uniform:

$$J(t) = \frac{j_0}{R}. \tag{7}$$

As for $\theta > 90°$, theoretical descriptions are rather complicated, and only a few can be found in the open literature. Popov [58] proposed the following analytical expression:

$$J(r,t) = \frac{j_0}{R}\left[\frac{1}{2}\sin\theta + \sqrt{2}(\cosh\eta + \cos\theta)^{\frac{3}{2}} \times \int_0^{\infty} \frac{\cosh\theta\zeta}{\cosh\pi\zeta}\tanh(\pi\zeta - \theta\zeta)P_{-\frac{1}{2}+i\zeta}(\cosh\eta)\zeta d\zeta\right], \tag{8a}$$

where $P_{-\frac{1}{2}+i\zeta}(x)$ are the Legendre functions of the first kind, and η is related to r as

$$r = \frac{R\sinh\eta}{\cosh\eta + \cos\theta}. \tag{8b}$$

However, this model is too complicated to get any analytical solution. Nguyen et al. [59] solved Eqs. (8a) and (8b) numerically by using Mathematica software, and found a suppression of evaporation near the contact edge. Although this model still requires further experimental validation, it will be used to calculate the evaporation flux distribution in this work.

2.3. Evaporation models within lBM framework

In order to embed the evaporation models into the LBM framework, we propose a scheme of reducing the order parameter ϕ at the interface every time step. When one defines ρ_L and ρ_G as the densities of the liquid and the gas, respectively, ϕ takes the minimum value $\phi_{min} = \frac{\rho_G - \rho_L}{2} = -\phi^* < 0$ in the gas region, the maximum value $\phi_{max} = \frac{\rho_L - \rho_G}{2} = \phi^* > 0$ in the liquid region, and zero across the interfacial region. Evaporation is assumed to take place only at the interface. If an interfacial lattice completely changes to a gas lattice in one time step (which means J/ρ_L equals the lattice speed, c) due to evaporation, then ϕ will change from $\phi(r,t)$ to $-\phi^*$, and the total change is $\phi(r,t) + \phi^*$.

For a real evaporation flux $J(r,t)$ at the interfacial lattice, the total change is

$$\Delta\phi(r,t) = (\phi(r,t) + \phi^*)\cdot\frac{J(r,t)}{c\rho_L}, \tag{9}$$

so that in the next time step,

$$\phi(r,t+\Delta t) = \phi(r,t) - (\phi(r,t) + \phi^*)\cdot\frac{J(r,t)}{c\rho_L}. \tag{10}$$

Note that $\phi(r,t)$ will not be reduced below $-\phi^*$ because the lattice speed c is always set at a very large value in our LBM scheme for fluid flows to insure the incompressible limit, and the real evaporation flux $J(r,t)$ is relatively much smaller. Thus, the evaporation regularities are introduced through the updating of interfacial ϕ after the streaming and collision process in each time step.

3. Results and discussion

3.1. Benchmarks

Our codes have been validated by three different test-cases. First, we check the model ability to deal with the high-density ratio in case of a static water drop on a solid surface in air. Second, the model accuracy is tested by modeling a drop falling along a vertical surface under gravity, and comparing with experimental data. Last, the evaporation scheme within the LBM framework is validated by modeling a standard liquid film evaporation case, and comparing with analytical solutions.

Consider water drops deposited on three substrates with different values of wettability which result in theoretical static contact angles at 45°, 90° and 135° respectively. The relative schematics are shown in Fig. 2. The initial shapes of the drops are all set as the same hemisphere with a radius equal to 80 Δx, where Δx is the lattice size. Gravity and evaporation are absent in this case, in order to test only the ability to model high-density ratios of the fluids and wettability. Other simulation parameters are listed in Table 1. We used the real densities of water and air, resulting into a density ratio over 800, while the kinematic viscosity ratio is about 15. Note that the lattice speed c is set at 50 m/s, large enough relative to the physical fluid velocity, which is less than 0.001 m/s, to ensure the incompressibility limit. After the systems reach the stationary state, the contact angles calculated for these three cases are 44.8°, 90.1° and 134.9° respectively, i.e. the maximum deviation from theoretical values is less than 0.45%. The good agreement of numerical and theoretical values thus validates our code for high density and viscosity ratios.

The second case is to let the water drop slide on a vertical wall under gravity. We compared our simulation results with experimental measurements in our laboratory. In the experiments, we

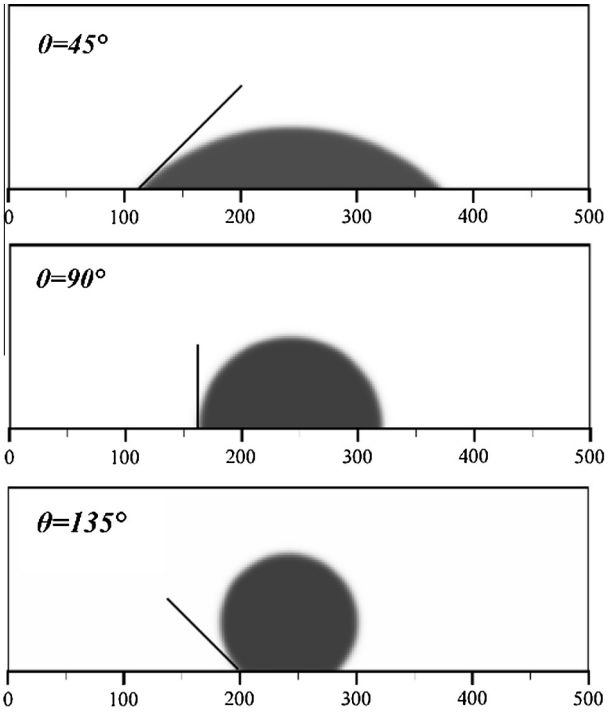

Fig. 2. Contact angles of static drops.

Table 1
Parameters for simulations.

Parameters	Values
Grid size	500×151
Droplet center position $\boldsymbol{x_c}$	250
Lattice size $\boldsymbol{\Delta x}$	2.5×10^{-5} m
Lattice speed $\boldsymbol{c}$	50 m/s
Liquid density $\boldsymbol{\rho_L}$	998.2 kg/m^3
Gas density $\boldsymbol{\rho_G}$	1.205 kg/m^3
Liquid kinetic viscosity $\boldsymbol{\nu_L}$	1.006×10^{-6} m^2/s
Gas kinetic viscosity $\boldsymbol{\nu_G}$	1.506×10^{-5} m^2/s
Surface tension $\boldsymbol{\sigma}$	0.072 N/m
Mobility $\boldsymbol{M}$	0.002 kg s/m^3
Interface width $\boldsymbol{W}$	3 Δx

let a deionized water drop slide on a vertical plastic wall under gravity. The movement of drops and the contact angles were measured by the Drop Shape Analysis system (DSA25, KRUSS) as shown in Fig. 3a. The images were obtained by a high speed CCD camera of 1000 fps. The solid wall is made of Polystyrene, and the static contact angle on a horizontal one for a deionized water drop was measured at 60° at the room temperature. Both the density and the viscosity of water and air were kept the same with our simulation.

Fig. 3(b) and (c) shows the comparison of the drop shapes obtained from the experiment and from the simulation when the drop shapes are changeless. We compared the drop base diameters, (3.71 mm from the experiment vs. 3.70 mm from the simulation), the advancing contact angles, (74.8° from the experiment vs. 72.4° from the simulation), and the receding contact angles, (45.6° from the experiment vs. 47.1° from the simulation). Such deviations are reasonably small enough to validate the ability of our code to describe drop movements under gravity. The deviation may be caused by different roughness status between simulations and experiments. In experiments the surface cannot be as perfectly smooth as supposed in simulations, which affects both the contact angle hysteresis and the viscous resistance.

Finally the evaporation scheme embedded in the lattice Boltzmann method was tested in a simple case of liquid film evaporation. Fig. 4 shows a rectangular liquid film with uniform evaporation on both the left and the right edges. The film had a surface area of 6 mm × 2 mm, which was discretized into 120 × 20 grid in modeling. Wetting properties at the top and the bottom boundaries were set by imposing a contact angle $\theta = 90°$. No gravity was considered here, while other parameters are the same as those in Table 1. When the uniform evaporation flux J is given, the total evaporation time t of the film can be calculated theoretically. The numerical results obtained for different values of J are compared with the corresponding analytical solutions in Table 2. The excellent agreement indicates that the evaporation scheme within the LBM framework is accurate.

3.2. Critical size for gravity impacts

After validations, our codes were used to quantitatively characterize the effect of gravity on water drops evaporating on a flat surface. It is well-known that as the drop size decreases, the surface-to-volume ratio becomes larger, which leads to a decrease of the ratio of gravity to the surface tension. As a result, the effect of gravity decreases with the drop size.

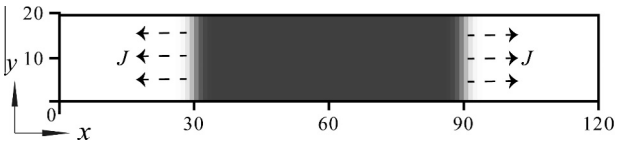

Fig. 4. Evaporation of liquid film with a uniform evaporation flux rate J.

Table 2
Comparisons between analytical solutions and modeling results for different J.

Evaporation flux J (kg/m^2 s)	Evaporation time t (s)		
	Analytical values	Simulation results	Deviations (%)
0.5	6	6.007	0.1
1	3	2.957	1.4
2	1.5	1.485	1.0
10	0.3	0.299	0.3

Initially, we compared the steady-state shapes of water drops under gravity at two different scales ($\Delta x = 0.025$ mm and $\Delta x = 0.0025$ mm), as illustrated in Fig. 5. Results show that when the drop size is small (the initial diameter of hemisphere is about 0.4 mm for $\Delta x = 0.0025$ mm), the drop shapes at equilibrium are spherical caps, i.e. they are determined by the surface tension. This means that gravity is negligible at this scale. When the drop size is enlarged ten times (the initial diameter is about 4 mm for $\Delta x = 0.025$ mm), the drop shape looks much flatter, deformed by gravity, hence gravity plays a key role at this scale and its effect is not negligible anymore. Note that evaporation is not considered yet at this stage. When a water drop evaporates, the drop size will decrease, and there must be a critical drop size below which gravity no longer influences the drop shape. As the capillary length ($L_c = \sqrt{\sigma/(\rho_l f_g)}$) is the empirical length scale which characterize the relative magnitudes of gravity and of the surface force, this length (or, more precisely, $2L_c$) has usually been considered as the critical drop size in the past and current literature, without further quantitative investigation.

To quantitatively determine the critical size of drops for which gravity can be neglected under various wetting conditions during the evaporation, the evaporation of water drops with different equilibrium contact angles ranging from 30° to 150° was modeled in grids with a lattice size $\Delta x = 0.025$ mm. Initial shapes before the

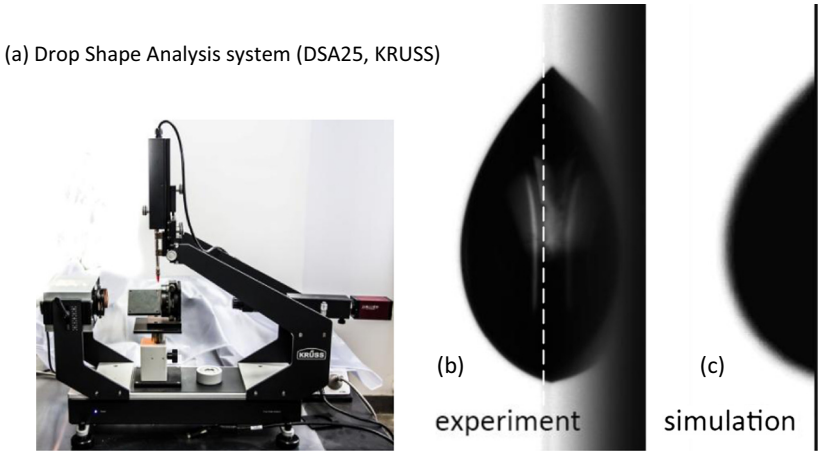

Fig. 3. Contact angles of sliding drops on vertical walls under gravity. The experiments were performed on DSA25, KRUSS in (a). The moving drop shape under a steady state from our experiments is shown in (b). (c) Shows the result from our simulations. In the experiments, deionized water drops slid under gravity on a vertical plastic wall. The white dashed line in (b) is a reference line of the drop bottom.

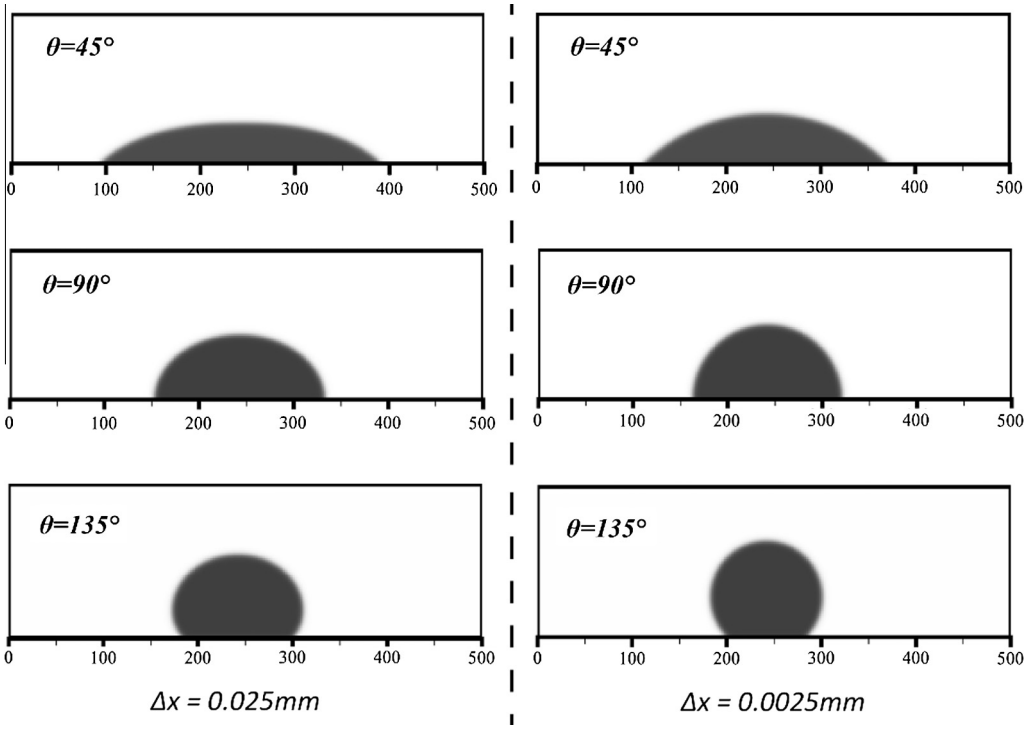

Fig. 5. Gravity effects on drop shape at two different scales for different contact angles. θ is the contact angle and Δx is the lattice size.

evaporation were set as their equilibrium shapes obtained from the same initial condition, i.e. a hemisphere with radius of 80Δ.

One straightforward way to capture the critical size is to compare the shape parameter of drops, i.e. the height to base diameter ratio h/d, with and without gravity. In theory, this ratio does not change for drops evaporating in the absence of gravity, while for drops under gravity, the relative importance of gravity with respect to surface tension decreases as the drop size decreases, so that the ratio h/d increases. As a result, the critical size can be found by comparing the h/d ratios of drops with and without gravity. Fig. 6 shows the results of such a comparison, where the simulation parameters are $\theta = 60°$ and $j_0 = 1 \times 10^{-3}$ kg/ms. One can find small fluctuations of the aspect ratio caused by removal of the evaporating components from the drops grid by grid. These fluctuations did not disappear with grid refinement (up to 4 times resolution compared with our early work [60]), especially those in the late stages of evaporation. Therefore fitting curves, a linear and a 2nd order polynomial ones, are adopted to determine the critical point. When the drop gets very small, e.g. $t > 2.0$ s in Fig. 6, the h/d ratio of drop increases even for the case without gravity, which may caused by limited grid number not enough to describe the shape of the drop. Therefore this method to determine the critical size will bring a large margin of error.

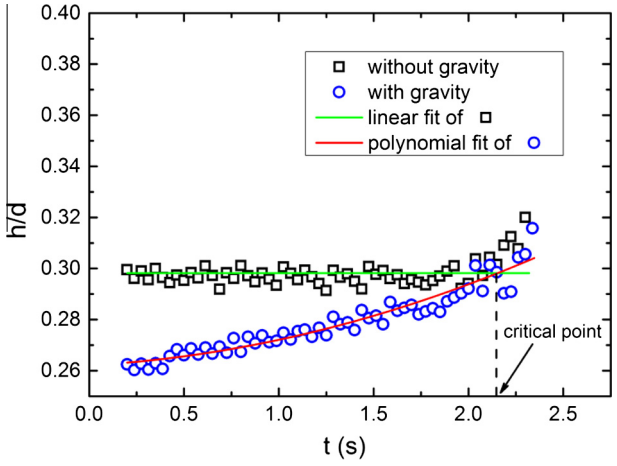

Fig. 6. Variations of h/d ratio vs. evaporate time.

An alternative method to identify the critical size is based on the analysis of the drop base diameter D_b during evaporation; this quantity exhibits a much smoother trend than the h/d ratio when plotted as a function of the evaporation time. Fig. 7(a) displays changing of the drop base diameter D_b with respect to time, comparing the cases with and without gravity. In this example, the evaporation parameters are the same as those in Fig. 6, i.e. $j_0 = 1 \times 10^{-3}$ kg/ms and the static contact angle is 60°. The base diameter D_b decreases as the sessile drop shrinks during evaporation. Fig. 7(a) also shows that in the case with gravity the base diameter is initially larger but decreases at a faster rate than in the case without gravity, so that the difference between the two trends eventually vanishes. The base diameter and its shrinking speed obviously related to the drop shape. For the same intrinsic contact angle (θ) and evaporation rate (j_0), the same shrinking speed of the base diameter D_b, means the same size and shape of drop. Therefore, comparing the drop base diameter in cases with and without gravity during evaporation allows one to determine the critical drop size relative to gravity effects.

In particular, one can fit the numerical values of the drop base diameter, displayed in Fig. 7(a), using analytical functions (e.g., 5th order polynomials), and then calculate the shrinking speed as the derivative of the fitting curves in the cases with and without gravity effects, as shown in Fig. 7(b). The two curves become asymptotic to each other as the drop evaporates and gets smaller (D_b decreases). Thus, one can set a threshold distance between the two curves below which they can be considered coincident. We have tried the value of 2%, 3% and 5%: for some cases, 2% is too hard to reach even if at the final moment; while for 5%, the

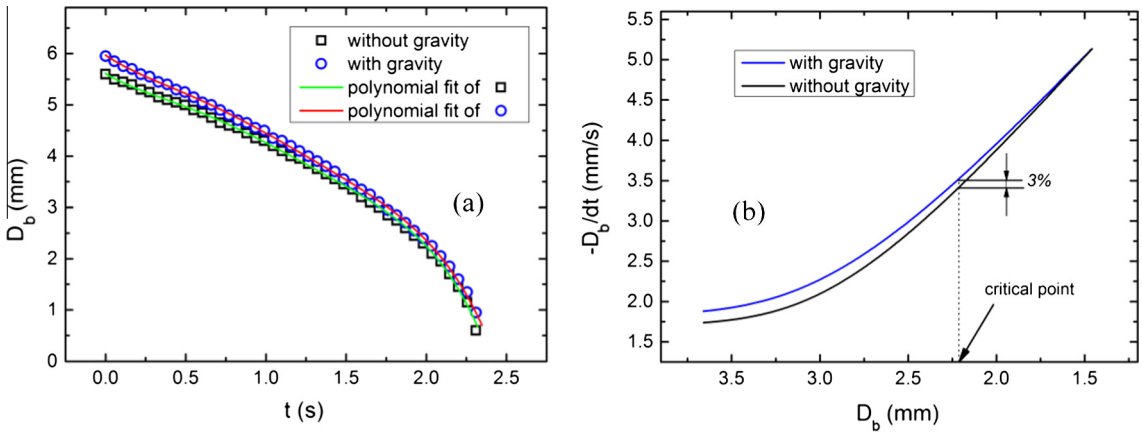

Fig. 7. Determination of the critical drop size from the contact line displacement. (a) Variations of the drop base diameter D_b vs. evaporation time t; (b) Slopes of the fitting curves $-dD_b/dt$ as functions of drop base diameter D_b.

shapes of the drops are still obviously affected by gravity; the critical drop size calculated using the threshold value of 3% is quantitatively consistent with that calculated using the drop shape criterion illustrated in Fig. 6. Therefore in Fig. 7, the threshold difference of 3% was adopted. If not mentioned specially, all the following results were calculated assuming the lines representative of the cases with and without gravity become coincident when their difference is 3%.

The critical drop size obtained using one of the above methods strongly depends on the contact angle. The effects of surface wettability and evaporation rate on the critical sizes of water drops are shown in Fig. 8, where the critical drop size is expressed using two different quantities: the base diameter D_b which is based on the contact area, and the effective diameter D_e which is the diameter of a sphere with the same water volume. While the former is easier to calculate and use, the latter can be more significant because it is not affected directly by the drop-surface interaction. Comparisons are made between the uniform evaporation mode and the non-uniform evaporation mode governed by Eqs. (6 and 7) with different values of j_0. Results show that the effect of the evaporation rate on the critical size is modest. For different surface wettabilities, the critical base diameter D_b decreases with increasing contact angle for drops with the same volume, because the contact angle dominates the drop shape under normal gravity. The critical effective diameter D_e exhibits a very different trend, depending on the surface wettability. When $\theta < 110°$, D_e keeps nearly constant (around 1 mm in the present example considering a water droplet), indicating that changing wettability hardly affect the droplet critical volume. However, D_e decreases for $\theta > 110°$. This could be explained in terms of the larger effect of gravity on taller drops at constant volume. In fact, a larger contact angle causes an increase of the drop height at the same water volume, so that one finds a decrease of D_e as a smaller critical size, indicating a larger effect of gravity. In addition, it is worth mentioning that the calculated values of D_e are generally much smaller than the classical capillary length (L_c) of water (2.7 mm), which denotes that many previous conclusions using the capillary length as critical size need reconsideration.

The correlation between the critical effective diameter, D_e, and the capillary length, L_c, has been studied by changing the gravitational acceleration, f_g. Results are shown in Fig. 9, where the simulation parameters are $\theta = 90°$ and $j_0 = 1 \times 10^{-3}$ kg/ms; these parameters were selected since D_e is constant when $\theta < 110°$ and nearly independent of evaporation condition. In this case, the linear correlation between the critical equivalent diameter and the capillary length is:

$$D_e = 0.4555 + 0.2115 L_c. \tag{11}$$

Since the initial effective diameter depends directly on the initial drop volume, this critical size together with the correlation, Eq. (11), can be a more exact indicator for experimental condition whether the gravity is negligible or not, except for some special

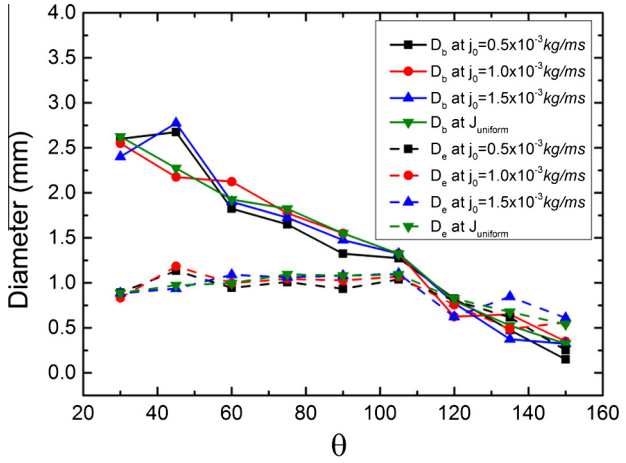

Fig. 8. Critical diameter vs. static contact angle θ under different evaporation conditions.

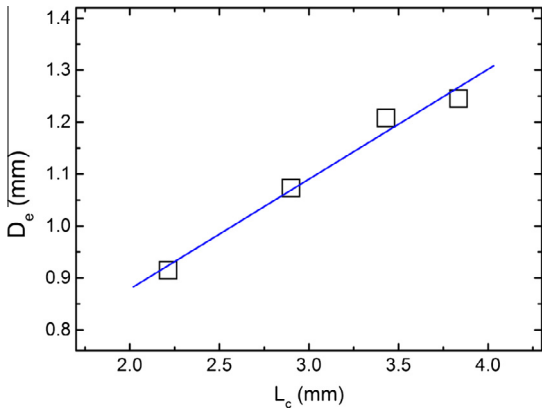

Fig. 9. Correlation between the critical effective diameter D_e and the capillary length L_c at $\theta = 90°$ and $j_0 = 1 \times 10^{-3}$ kg/ms. Squares represent the results of simulations and the line is their linear best-fit.

surface treatments for super-hydrophobic properties [61]. We believe that the fluid properties, including viscosity, density, surface tension and so on, will change the critical drop size more or less, but since in this work we focus on water drops and demonstrating the capabilities of our method, more efforts will be made to consider other properties or fluids.

4. Conclusions

A multiphase LBM model for large density ratio was used to investigate the evaporation of water drops deposited on a horizontal substrate. To account for physically consistent evaporation criteria within the framework of LBM, a novel evaporation scheme was also introduced. Both the LBM code and the evaporation scheme were validated in three simple test cases, either with theoretical solutions or with experimental measurements.

The steady state shapes of droplets with two different scales under normal gravity were compared, confirming that the effect of gravity vanishes at smaller drop sizes. To identify the effects of gravity, simulations were run with and without gravity force under different conditions of wettability and evaporation rate. It was found that the differences between the cases with and without gravity reduce as drops evaporate, which confirms the effect of gravity becomes negligible at smaller sizes. This allows one to identify a critical size of water droplets under which gravity can be neglected; in particular, such critical drop size is expressed in terms of an equivalent drop diameter. Results show that all the calculated values of the critical diameter are significantly smaller than the capillary length, which is commonly used as a reference for the critical drop size; thus, many previous studies may need reconsideration. Moreover, this critical diameter is found to be independent of the evaporation conditions, and constant with respect to the surface wettability, to the exclusion of highly hydrophobic (and super-hydrophobic) cases. Therefore, it could be a more reliable indicator of gravity effects than the classical capillary length. Finally, a linear correlation between this critical diameter and the capillary length was provided for easier application of the results.

Acknowledgments

This work is financially supported by the NSF Grant of China (No. 51176089), the Specialized Research Fund for the Doctoral Program of Higher Education of China (No. 20130002110077) and Tsinghua University Initiative Scientific Research Program (No. 2014z22074).

References

[1] V. Mironov, T. Boland, T. Trusk, G. Forgacs, R.R. Markwald, Trends Biotechnol. 21 (2003) 157.
[2] V. Bertola, Int. J. Heat Mass Transfer 85 (2015) 430.
[3] R.D. Deegan, O. Bakajin, T.F. Dupont, G. Huber, S.R. Nagel, T.A. Witten, Nature 389 (1997) 827.
[4] R.D. Deegan, Phys. Rev. E 61 (2000) 475.
[5] R.D. Deegan, O. Bakajin, T.F. Dupont, G. Huber, S.R. Nagel, T.A. Witten, Phys. Rev. E 62 (2000) 756.
[6] L. Malaquin, T. Kraus, H. Schmid, E. Delamarche, H. Wolf, Langmuir 23 (2007) 11513.
[7] V. Dugas, J. Broutin, E. Souteyrand, Langmuir 21 (2005) 9130.
[8] T.-S. Wong, T.-H. Chen, X. Shen, C.-M. Ho, Anal. Chem. 83 (2011) 1871.
[9] S. Semenov, V.M. Starov, M.G. Velarde, R.G. Rubio, Eur. Phys. J. Spec. Top. 197 (2011) 265.
[10] R.G. Picknett, R. Bexon, J. Colloid Interface Sci. 61 (1977) 336.
[11] J.-H. Kim, S.I. Ahn, J.H. Kim, W.-C. Zin, Langmuir 23 (2007) 6163.
[12] D. Brutin, Z. Zhu, O. Rahli, J. Xie, Q. Liu, L. Tadrist, Microgravity Sci. Technol. 21 (2009) 67.
[13] D. Brutin, B. Sobac, Phys. Rev. E 86 (2012) 021602.
[14] B.J. Fischer, Langmuir 18 (2001) 60.
[15] E. Bonaccurso, H.-J.R. Butt, J. Phys. Chem. B 109 (2004) 253.
[16] S. Cioulachtjian, S. Launay, S. Boddaert, M. Lallemand, Int. J. Therm. Sci. 49 (2010) 859.
[17] H.Y. Erbil, R.A. Meric, J. Phys. Chem. B 101 (1997) 6867.
[18] X. Fang, B. Li, E. Petersen, Y. Ji, J.C. Sokolov, M.H. Rafailovich, J. Phys. Chem. B 109 (2005) 20554.
[19] G. Guéna, C. Poulard, M. Voué, J. De Coninck, A.M. Cazabat, Colloids Surf. A: Physicochem. Eng. Aspects 291 (2006) 191.
[20] Y. Takata, S. Hidaka, A. Yamashita, H. Yamamoto, Int. J. Heat Fluid Flow 25 (2004) 320.
[21] H. Gelderblom, Á.G. Marín, H. Nair, A. van Houselt, L. Lefferts, J.H. Snoeijer, D. Lohse, Phys. Rev. E 83 (2011) 026306.
[22] B. Sobac, D. Brutin, Langmuir 27 (2011) 14999.
[23] G. McHale, S. Aqil, N.J. Shirtcliffe, M.I. Newton, H.Y. Erbil, Langmuir 21 (2005) 11053.
[24] C.-H. Choi, C.-J.C.J. Kim, Langmuir 25 (2009) 7561.
[25] X. Zhang, S. Tan, N. Zhao, X. Guo, X. Zhang, Y. Zhang, J. Xu, ChemPhysChem 7 (2006) 2067.
[26] X. Chen, R. Ma, J. Li, C. Hao, W. Guo, B.L. Luk, S.C. Li, S. Yao, Z. Wang, Phys. Rev. Lett. 109 (2012) 116101.
[27] M. Cachile, O. Bénichou, C. Poulard, A.M. Cazabat, Langmuir 18 (2002) 8070.
[28] H. Hu, R.G. Larson, J. Phys. Chem. B 106 (2002) 1334.
[29] H. Hu, R.G. Larson, Langmuir 21 (2005) 3963.
[30] G.J. Dunn, S.K. Wilson, B.R. Duffy, S. David, K. Sefiane, J. Fluid Mech. 623 (2009) 329.
[31] R. Teshigawara, A. Onuki, EPL (Europhys. Lett.) 84 (2008) 36003.
[32] E. Widjaja, M.T. Harris, Comput. Chem. Eng. 32 (2008) 2169.
[33] J. Zhang, F. Leroy, F. Müller-Plathe, Langmuir 29 (2013) 9770.
[34] V.K. Badam, F. Durst, C.A. Ward, F. Duan, Phys. Rev. E 72 (2005) 056303.
[35] F. Duan, C.A. Ward, Langmuir 25 (2009) 7424.
[36] C.A. Ward, H. Ghasemi, Phys. Rev. Lett. 105 (2010) 136102.
[37] H. Hu, R.G. Larson, J. Phys. Chem. B 110 (2006) 7090.
[38] M. Majumder, C.S. Rendall, J.A. Eukel, J.Y.L. Wang, N. Behabtu, C.L. Pint, T.-Y. Liu, A.W. Orbaek, F. Mirri, J. Nam, A.R. Barron, R.H. Hauge, H.K. Schmidt, M. Pasquali, J. Phys. Chem. B 116 (2012) 6536.
[39] A.-M. Cazabat, G. Guena, Soft Matter 6 (2010) 2591.
[40] S. Chen, G.D. Doolen, Annu. Rev. Fluid Mech. 30 (1998) 329.
[41] C.K. Aidun, J.R. Clausen, Annu. Rev. Fluid Mech. 42 (2010) 439.
[42] M. Wang, Q. Kang, Anal. Chem. 81 (2009) 2953.
[43] M. Wang, J. Heat Transfer 134 (2012) 051020.
[44] A.K. Gunstensen, D.H. Rothman, S.P. Zaleski, G. Zanetti, Phys. Rev. A 43 (1991) 4320.
[45] A.K. Gunstensen, D.H. Rothman, J. Geophys. Res. 98 (1993) 6431.
[46] X. Shan, H. Chen, Phys. Rev. E 47 (1993) 1815.
[47] Q. Kang, D. Zhang, S. Chen, Phys. Fluids 14 (2002) 3203.
[48] M.R. Swift, W.R. Osborn, J.M. Yeomans, Phys. Rev. Lett. 75 (1995) 830.
[49] X. He, S. Chen, G.D. Doolen, J. Comput. Phys. 146 (1998) 282.
[50] X. He, S. Chen, R. Zhang, J. Comput. Phys. 152 (1999) 642.
[51] H.W. Zheng, C. Shu, Y.T. Chew, J. Comput. Phys. 218 (2006) 353.
[52] T. Inamuro, T. Ogata, S. Tajima, N. Konishi, J. Comput. Phys. 198 (2004) 628.
[53] T. Inamuro, Fluid Dyn. Res. 38 (2006) 641.
[54] A.S. Joshi, Y. Sun, J. Display Technol. 6 (2010) 579.
[55] Y. Sun, A.S. Joshi, Phys. Rev. E 82 (2010) 041401.
[56] Y. Morozumi, in: Proceedings of International Conference on Chemistry and Chemical Engineering (ICCCE 2011), 2011.
[57] J.W. Cahn, J.E. Hilliard, J. Chem. Phys. 28 (1958) 258.
[58] Y.O. Popov, Phys. Rev. E 71 (2005) 036313.
[59] T.A.H. Nguyen, A.V. Nguyen, M.A. Hampton, Z.P. Xu, L. Huang, V. Rudolph, Chem. Eng. Sci. 69 (2012) 522.
[60] C. Xie, J. Zhang, M. Wang, Appl. Math. Mech. 35 (2014) 247.
[61] Y.H. Liu, L. Moevius, X.P. Xu, T.Z. Qian, J.M. Yeomans, Z.K. Wang, Nat. Phys. 10 (2014) 515.